Development of a Quasi-static Particle-in-Cell Code for Nonlinear Beam-Driven Plasma Wakefield Acceleration: Progress Report

Gangtak N.[1], Hemba E. C.[2], Akila S.[3] and Timchang C.[4]
[1,2,3&4]*Department of Physics, Federal College of Education Pankshin Nigeria*

Abstract: This work introduces a quasi-static PIC code tailored for simulating nonlinear beam-driven PWFAs, leveraging the quasi-static approximation to reduce computational overhead by removing stringent time step constraints inherent in explicit PIC methods. The methodology involves constructing numerical plasma macro-particle distributions, calculating charge and current densities, and integrating electromagnetic field components through Poisson-like equations solved via fast Poisson solvers. An iterative predictor-corrector scheme based on the Adams-Bashforth-Moulton method ensures precise advancement of plasma particles. The beam particles are advanced using a relativistic Lorentz force equation to accommodate high-velocity dynamics. Preliminary simulations demonstrate the code's effectiveness in representing highly localized and focused beam densities, which are suitable for strong wakefield generation. Charge and current density distributions exhibit uniformity with localized perturbations, aligning with theoretical expectations for wakefield excitation. These results validate the code's capability to accurately capture the complex dynamics of beam-plasma interactions with enhanced computational efficiency. This progress report highlights the developed quasi-static PIC code as a robust tool for advancing PWFA research. By significantly reducing computational demands without compromising simulation accuracy, the code facilitates more extensive investigations into plasma-based acceleration mechanisms. Future work will focus on comprehensive validation against experimental data, optimizing computational performance, and integrating additional physical phenomena to further enhance the simulation framework.

I INTRODUCTION

The potential of plasma accelerators to generate ultrahigh accelerating gradients and facilitate substantial energy transfer has been extensively documented (Litos et al., 2016; Gangtak et al., 2016; Massimo et al., 2013; Haruna and Anchaver, 2013; Diederichs et al., 2022; Gangtak et al., 2017). Despite their advantages over conventional particle colliders, realizing plasma-based accelerators remains challenging, as highlighted by Diederichs et al. (2022), who emphasize that "significant advances are still required to make plasma-accelerator-driven applications feasible."

Accurate prediction of beam-plasma dynamics requires computationally expensive full electromagnetic particle-in-cell (PIC) codes (Petri et al., 2017). However, exploring and improving plasma accelerators necessitates efficient computational tools (Zgadzaj et al., 2020). Pukhov (2015) demonstrated that quasi-static codes, utilizing quasi-static approximation techniques, require fewer computational resources than explicit PIC codes and Lorentz boosted codes, due to the elimination of the time step restriction imposed by the Courant-Friedrich-Lewy condition. This finding supports the adoption of quasi-static approximation techniques in this work.

The evolving landscape of plasma wakefield acceleration (PWFA) research demands innovative numerical approaches to address emerging challenges and explore new opportunities (US Dept. of Energy, 2016; UK Roadmap for PWFA Research, 2019). This work presents the development of a quasi-static PIC code for simulating nonlinear beam-driven PWFA. The code is designed to capture complex beam-plasma interactions, enabling precise and efficient simulation of PWFA.

This document outlines the code development process, including numerical methods, algorithms, and beam-plasma configurations used. The goal is to promote innovative numerical tools tailored for PWFA research.

II METHOD OF SOLUTION

A *Numerical Plasma Macro-Particle Distribution*

The plasma distribution function can be expressed as a collection of finite-sized macro particles (Lapenta, 2015), of the form

$$f(x,p,t) = \sum_n^N S_r\left(r - r_\varphi(t)\right) S_p\left(p - p_\varphi(t)\right) \quad (1)$$

But we are interested in the quasi-static approximation PIC model, therefore the new set of coordinates $(x, y, s = z, \xi = t)$ will replace the set of coordinates (x, y, z, t) used in explicit PIC code. Where $\xi = ct - z$ is the embedded time parameter and $s = z$, represents the propagation distance travelled in plasma by the drive beam. So that equation (1) will then become

$$f(x,p,\xi) = \sum_n^N S_r\left(r - r_\varphi(\xi)\right) S_p\left(p - p_\varphi(\xi)\right) \quad (2)$$

For computational convenience, we will use the first order shape function

$$S\left(x - x_\varphi(\xi)\right) = S_i(x) = \begin{cases} 1 - \frac{|x - x_\varphi|}{\Delta x}, & |x - x_\varphi| \le \frac{\Delta x}{2} \\ 0, & |x - x_\varphi| > \frac{\Delta x}{2} \end{cases} \quad (3)$$

also

$$S_j(y) = \begin{cases} 1 - \frac{|y - y_\varphi|}{\Delta y}, & |y - y_\varphi| \le \frac{\Delta y}{2} \\ 0, & |y - y_\varphi| > \frac{\Delta y}{2} \end{cases} \quad (4)$$

$$S_k(z) = \begin{cases} 1 - \frac{|z - z_\varphi|}{\Delta z}, & |z - z_\varphi| \le \frac{\Delta z}{2} \\ 0, & |z - z_\varphi| > \frac{\Delta z}{2} \end{cases} \quad (5)$$

The macro particle shape function $S\left(r - r_\varphi(\xi)\right)$ is related to the macro particle weighting function w_i by setting $r = r_i$ (i.e. $r(x,y,z) = r_i(x_i, y_j, z_k)$), where r_i represents the grid coordinate of the macro particles. Therefore, it can be implied that

$$S\left(r_i - r_\varphi(\xi)\right) = w_i\left(r_i - r_\varphi(\xi)\right) \quad (6)$$

in that the plasma macro-particle interpolation onto the grid points (i.e. assignment of macro particles to grid points) can be possible through the use of the macro particle weighting function

$$w_i(x_\varphi) = \frac{x_{i+1} - x_\varphi}{\Delta x} \quad (7)$$

and

$$w_{i+1}(x_\varphi) = \frac{x_\varphi - x_i}{\Delta x} \quad (8)$$

where x_φ represents the macro particles positions or coordinates, x_i and x_{i+1} are the grid coordinates or quantities. From equation (7) and (8), the macro particles distribution on the grid can be established. Also

$$w_j(y_\varphi) = \frac{y_{j+1} - y_\varphi}{\Delta y} \quad (9)$$

and

$$w_{j+1}(y_\varphi) = \frac{y_\varphi - y_j}{\Delta y} \quad (10)$$

as well as

$$w_k(z_\varphi) = \frac{z_{k+1} - z_\varphi}{\Delta z} \quad (11)$$

$$w_{k+1}(z_\varphi) = \frac{z_\varphi - z_k}{\Delta z} \quad (12)$$

where $x_{i+1} = \Delta x - x_i$, $y_{j+1} = \Delta y - y_j$, and $z_{k+1} = \Delta z - z_k$.

A 3D version of the shape function can then be expressed as

$$S\left(r - r_\varphi(\xi)\right) = S_i(x_\varphi) S_j(y_\varphi) S_k(z_\varphi) \quad (13)$$

Similarly, the weighting function will be

$$w_{i,j,k}\left(r_{i,j,k} - r_\varphi(\xi)\right) = w_i(x_\varphi) w_j(y_\varphi) w_k(z_\varphi) \quad (14)$$

Next, the number of macro-particles representing the plasma particle species is distributed on the grid according to

$$N = \sum_{n=1}^{N_s} w_{i,j,k}\left(r_{i,j,k} - r_\varphi(\xi)\right) = N_s \quad (15)$$

and the number density of the macro particles representing the plasma particle species density on the grid follows the model (Wojciech, 2017)

$$n_{p_s} = \sum_{n=1}^{N_s} w_{i,j,k}\left(r_{i,j,k} - r_\varphi(\xi)\right) = N_s \quad (16)$$

where $\sum w_{i,j,k}\left(r_{i,j,k} - r_\varphi(\xi)\right) = 1$. Therefore, the macro particles that will be assigned to the grid points using $w_i(x_\varphi)$, $w_j(y_\varphi)$, $w_k(z_\varphi)$ and $w_{i+1}(x_\varphi)$, $w_{j+1}(y_\varphi)$, $w_{k+1}(z_\varphi)$ can be expressed as

$$N\left(r_{i,j,k}, r_\varphi(\xi)\right) = N_s\left[\frac{x_{i+1} - x_\varphi}{\Delta x}, \frac{y_{j+1} - y_\varphi}{\Delta y}, \frac{z_{k+1} - z_\varphi}{\Delta z}\right] \quad (17)$$

and

$$N\left(r_{i+1,j+1,k+1}, r_{\varphi}(\xi)\right) = N_s\left[\frac{x_{\varphi}-x_i}{\Delta x}, \frac{y_{\varphi}-y_j}{\Delta y}, \frac{z_{\varphi}-z_k}{\Delta z}\right] \quad (18)$$

In the same way, the macro particle number density, representing plasma particle species density can also be written in the form of equation (17) and (18).

B *Plasma Charge and Current Density*

Now, the plasma charge density, viewed as charge per unit volume can be expressed as

$$\rho(r,\xi) = \frac{1}{\Delta V}\sum_{\varphi=1}^{N_s} q_T \gamma_p S_r\left(r - r_{\varphi}(\xi)\right)$$

or it can be expressed using the macro particle weighting or interpolation function as

$$\rho(r,\xi) = \frac{1}{\Delta V}\sum_{\varphi=1}^{N_s} q_T \gamma_p\, w_{ijk}\left(r_{ijk} - r_{\varphi}(\xi)\right) \quad (19)$$

Therefore, the charge density interpolated or assigned to the grid points (i,j,k) can then be

$$\rho_{s_{ijk}}(r,\xi) = \frac{Q_{s_{ijk}}(\xi)}{V_{i,j,k}}\frac{1}{V_{ijk}}\sum_{\varphi=1}^{N_s} q_T \gamma_{p\varphi}\, w_{ijk}\left(r_{ijk} - r_{\varphi}(\xi)\right) \quad (20)$$

Where $q_{T_{ijk}} = \sum_{\varphi=1}^{N_s}\frac{q_{\varphi_{ijk}}mc^2}{mc^2+q_{\varphi_{ijk}}\psi_{ijk}}$ is the cumulative charge species in a cell and $\gamma_{p\varphi}$is the Lorentz factor associated with the particle and is presented as

$$\gamma_{p\varphi} = \frac{1+\frac{p_r^2}{m^2c^2}+\left(1+\frac{q\varphi\psi}{mc^2}\right)^2}{2\left(1+\frac{q\varphi\psi}{mc^2}\right)} \text{ or}$$

$$\gamma_{p\varphi} = \frac{1+\frac{u_r^2}{c^2}+\left(1+\frac{q\varphi\psi}{mc^2}\right)^2}{2\left(1+\frac{q\varphi\psi}{mc^2}\right)} \quad (21)$$

where $u = \gamma v$ has been used.

The plasma macro particle current density scheme can also be represented as

$$J_p(r,\xi) = \frac{1}{\Delta V}\sum_{\varphi=1}^{N_s} q_T u_{\varphi} S_r\left(r - r_{\varphi}(\xi)\right) \quad (22)$$

It can also be assigned or interpolated to grid points through the use of the weighting function as

$$J_{p_{ijk}}(r,\xi) = \frac{1}{V_{ijk}}\sum_{\varphi=1}^{N_s} q_T u_{\varphi} w\left(r_{ijk} - r_{\varphi}(\xi)\right) \quad (23)$$

C *Charge Density, Current Density and Electromagnetic Field Components Relation to their Source term*

Using quasi-static approximation, the charge and current density sources will be

$$\nabla_r^2\phi = -4\pi\rho(x,y,\xi,s) \quad (24)$$

$$\nabla_r^2 A = -\frac{4\pi}{c}J(x,y,\xi,s) \quad (25)$$

Equation (25) can be rewritten in term of the longitudinal and transverse current density as

$$\nabla_r^2 A_z = -\frac{4\pi}{c}J_z(x,y,\xi,s) \quad (26)$$

$$\nabla_r^2 A_r = -\frac{4\pi}{c}J_r(x,y,\xi,s) \quad (27)$$

Next, we will transform equation (26) and (27) to suit our electromagnetic field source terms. To achieve this, we start by taking the derivative of equation (27) as

$$\nabla_r^2\frac{\partial A_r}{\partial\xi} = -\frac{4\pi}{c}\frac{\partial J_r}{\partial\xi} \quad (28)$$

At this stage, the Lorentz gauge - $\nabla_r \cdot A_r = -\frac{\partial\psi}{\partial\xi}$ can be solved to obtain

$$A_r = -r\frac{\partial\psi}{\partial\xi} \quad (29)$$

From equation (29) we can also have

$$\frac{\partial A_r}{\partial\xi} = -r\frac{\partial^2\psi}{\partial\xi^2} = -r\frac{\partial E_z}{\partial\xi} \quad (30)$$

By substituting equation (30) into (28), we get

$$\nabla_r^2\frac{\partial E_z}{\partial\xi} = -\frac{4\pi}{rc}\frac{\partial J_r}{\partial\xi} \quad (31)$$

Also, we will quantify the vector potential A_z using the relation

$$A_z(\xi,r) = \lambda(\xi)\ln r \quad (32)$$

within the blowout region where $r \le r_b$. Since $\ln r$ is the same as e^{-r} (i.e. $\ln r = e^{-r}$), then equation (32) can be written as

$$A_z(\xi, r) = \lambda(\xi)e^{-r} \quad (33)$$

And by differentiating equation (33), we get

$$\frac{\partial A_z}{\partial r} = -\lambda(\xi)e^{-r} \quad (34)$$

From equation (26), we can have

$$\nabla_r^2 \frac{\partial A_z}{\partial r} = -\frac{4\pi}{c}\frac{\partial J_z}{\partial r} \quad (35)$$

By plugging equation (34) into (35), we can have

$$\nabla_r^2\lambda(\xi) + \lambda(\xi) = \frac{4\pi e^r}{c}\frac{\partial J_z}{\partial r} \quad (36)$$

Also, from equation (29) and (33), we can express equation (26) and (27) as

$$\nabla_r^2 \frac{\partial \psi}{\partial \xi} = \frac{4\pi}{rc}J_r(x, y, \xi, s) \quad (37)$$

or

$$\nabla_r^2 E_z = \frac{4\pi}{rc}J_r(x, y, \xi, s) \quad (38)$$

and

$$\nabla_r^2\lambda(\xi) + \lambda(\xi) = -\frac{4\pi}{c}e^r J_z(x, y, \xi, s) \quad (39)$$

Using equation (37), we can have

$$\frac{\partial}{\partial \xi}\nabla_r^2\psi = \frac{4\pi}{c}J_r(x, y, \xi, s) \quad (40)$$

From the relation $\nabla_r^2\psi = -(\rho - J_z)$, we can cast equation (40) as

$$\frac{\partial}{\partial \xi}(\rho - J_z) = -J_r(x, y, \xi, s) \quad (41)$$

Using the continuity equation form in quasi static approximation model, we can have

$$\frac{\partial}{\partial \xi}(\rho - J_z) = -\nabla_r \cdot J_r(x, y, \xi, s) \quad (42)$$

Comparing equation (41) and (42), we get

$$J_r(x, y, \xi, s) = \nabla_r \cdot J_r(x, y, \xi, s) \quad (43)$$

Substituting equation (43) into (38), we get

$$\nabla_r^2 E_z = \frac{4\pi}{rc}\nabla_r \cdot J_r(x, y, \xi, s) \quad (44)$$

So far, it evident that we need to specify $\frac{\partial J_z}{\partial r}$ and $\frac{\partial J_r}{\partial \xi}$. To achieve this, the current density will be rewritten as

$$J_r(\xi, r) = \frac{1}{\Delta V}\sum_{\varphi=1}^{N}\frac{q_\varphi mc^2 u_{r\varphi}}{mc^2 + q_\varphi\psi}S_r\left(r - r_\varphi(\xi)\right) \quad (45)$$

$$J_z(\xi, r) = \frac{1}{\Delta V}\sum_{\varphi=1}^{N}\frac{q_\varphi mc^2 u_{z\varphi}}{mc^2 + q_\varphi\psi}S_r\left(r - r_\varphi(\xi)\right) \quad (46)$$

By differentiating equation (384) with respect to ξ, we get

$$\frac{\partial}{\partial \xi}J_r(\xi, r) = \frac{1}{\Delta V}$$

$$\left\{\sum_{\varphi=1}^{N} q_T\frac{\partial u_{r\varphi}}{\partial \xi}S_r\left(r - r_\varphi(\xi)\right) - \sum_{\varphi=1}^{N}\frac{q_T^2 u_{r\varphi}}{mc^2}\frac{\partial \psi}{\partial \xi}S_r\left(r - r_\varphi(\xi)\right) - \sum_{\varphi=1}^{N} q_T u_{r\varphi}\frac{\partial r_\varphi(\xi)}{\partial \xi}S_r\left(r - r_\varphi(\xi)\right)\right\} \text{ or}$$

$$\frac{\partial}{\partial \xi}J_r(\xi, r) = \frac{1}{\Delta V}\sum_{\varphi=1}^{N} q_T S_r\left(r - r_\varphi(\xi)\right)\left\{\frac{\partial u_{r\varphi}}{\partial \xi} - \frac{q_T u_{r\varphi}}{mc^2}\frac{\partial \psi}{\partial \xi} - u_{r\varphi}\frac{\partial r_\varphi(\xi)}{\partial \xi}\right\} \quad (47)$$

Similarly, differentiating equation (45) w. r. t. r, we get

$$\frac{\partial}{\partial r}J_z(\xi, r) = \frac{1}{\Delta V}\sum_{\varphi=1}^{N}\frac{q_\varphi mc^2 u_{z\varphi}}{mc^2 + q_\varphi\psi}S_r\left(r - r_\varphi(\xi)\right) = \frac{1}{\Delta V}\sum_{\varphi=1}^{N} q_T u_{z\varphi} S_r\left(r - r_\varphi(\xi)\right) \quad (48)$$

$$\frac{\partial}{\partial r}J_r(\xi, r) = \frac{1}{\Delta V}\sum_{\varphi=1}^{N} q_T u_{r\varphi} S_r\left(r - r_\varphi(\xi)\right) \quad (49)$$

One can observe that $\frac{\partial}{\partial r}J_z(\xi, r) = J_z(\xi, r)$. Using Maxwell's equations expressed in terms of the variable ξ,

$$\nabla \cdot E = 4\pi\rho \quad (50)$$

$$\nabla \cdot B = 0 \quad (51)$$

$$\frac{\partial B}{\partial \xi} = \nabla \times E \quad (52)$$

$$\nabla \times B = -\frac{\partial E}{\partial \xi} + \frac{4\pi}{c}J \quad (53)$$

we can show how the radial electric field and magnetic field component relates with charge and current densities. Therefore, by taking the curl of equation (53), will lead to

$$\nabla(\nabla \cdot B) - \nabla_r^2 B = -\frac{\partial}{\partial \xi}\nabla_r \times E_r + \frac{4\pi}{c}\nabla_r \times J_z \quad (54)$$

Clearly, $\frac{\partial}{\partial \xi}\nabla_r \times E_r = 0$ and using equation (51), (54) will reduce to the form

$$\nabla_r^2 B = -\frac{4\pi}{c}\nabla_r \times J_z \text{ or}$$

$$\nabla_r^2 B = -\frac{4\pi}{c}\left(\frac{\partial}{\partial x}J_z - \frac{\partial}{\partial y}J_z\right) \quad (55)$$

We can rewrite equation (55) as

$$\nabla_r^2 B = -\frac{4\pi}{c}\left[\frac{\partial}{\partial x}\left(J_z - \frac{\partial E_z}{\partial \xi}\right) - \frac{\partial}{\partial y}\left(J_z - \frac{\partial E_z}{\partial \xi}\right)\right] \quad (56)$$

since $\frac{\partial}{\partial x}\left(\frac{\partial E_z}{\partial \xi}\right) = 0$. Equation (56) can be separated as

$$\nabla_x^2 B = -\frac{4\pi}{c}\frac{\partial}{\partial x}\left(J_z - \frac{\partial E_z}{\partial \xi}\right) \quad (57)$$

$$\nabla_y^2 B = \frac{4\pi}{c}\frac{\partial}{\partial y}\left(J_z - \frac{\partial E_z}{\partial \xi}\right) \quad (58)$$

By taking the curl of equation (52), will lead to

$$\frac{\partial}{\partial \xi}\nabla \times B = \nabla_r(\nabla_r \cdot E_r) - \nabla_r^2 E_r \quad (59)$$

Using equations (50) and (53), equation (59) will become

$$\nabla_r^2 E_r = \frac{4\pi}{c}\left(c\nabla_r \rho - \frac{\partial J_r}{\partial \xi}\right) \quad (60)$$ because E_r is independent of ξ and therefore $\frac{\partial^2 E_r}{\partial \xi^2} = 0$. It can also be observed that equations (31), (36), (44), (57), (58) and (60) are Poisson-like equations that can be solved using fast Poisson solvers. Aside these field equations, we also need the wakefield potential ψ.

Lastly, substitute equation (47) into (60) and (31) to arrive at

$$\nabla_r^2 E_r = 4\pi\nabla_r \rho - \frac{4\pi}{c\Delta V}\sum_{\varphi=1}^{N} q_T S_r\left(r - r_\varphi(\xi)\right)\left\{\frac{\partial u_{r\varphi}}{\partial \xi} - \frac{q_T}{mc^2}u_{r\varphi}\frac{\partial \psi}{\partial \xi} - q_T u_{r\varphi}^2\right\} \quad (61)$$

$$\nabla_r^2 \frac{\partial E_z}{\partial \xi} = \frac{4\pi}{rc\Delta V}\sum_{\varphi=1}^{N} q_T S_r\left(r - r_\varphi(\xi)\right)\left\{\frac{\partial u_{r\varphi}}{\partial \xi} - \frac{q_T}{mc^2}u_{r\varphi}\frac{\partial \psi}{\partial \xi} - q_T u_{r\varphi}^2\right\} \quad (62)$$

D *The Quasi Static PIC Algorithm*

The flow chart below illustrates the quasi-static particle-in-cell algorithm implemented, where the initialized beam particles distribution, plasma particles distribution, charge and current density distributions representation are presented.

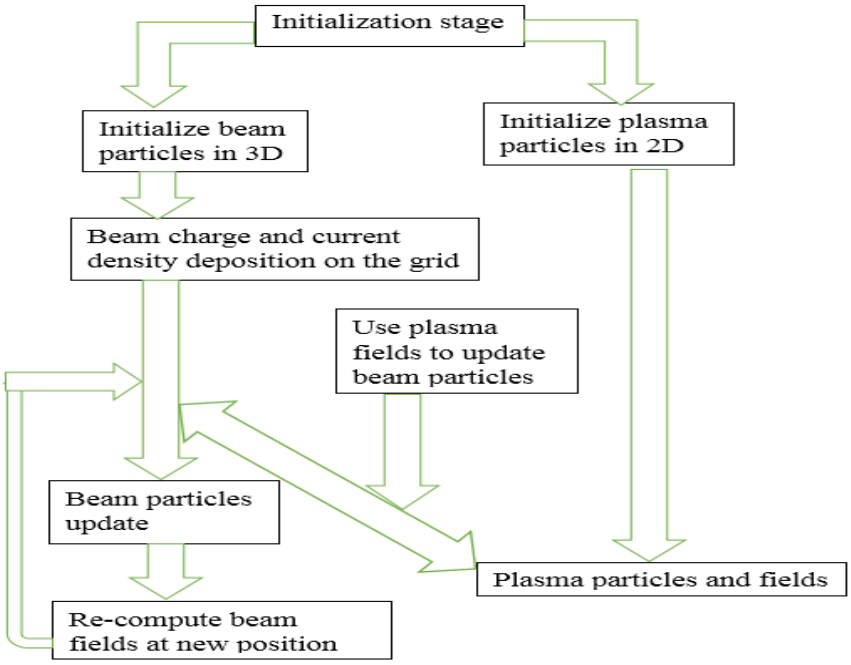

Figure 1: flow chart of the basic quasi static algorithm

Now, the computation of these electromagnetic field components at grid points using numerical schemes can be demonstrated. As such, the flow chart below illustrates the iterative predictor-corrector scheme required for fields and particles deposition implemented. First, the macro-particles position and velocity are prediction, which is then followed charge and current density deposition as grid points, next is computation of electromagnetic field components where the macro-particles positions and velocity will be updated at new positions, so the charge and current density will be corrected and new electromagnetic field components will be recomputed until the specified condition is attained.

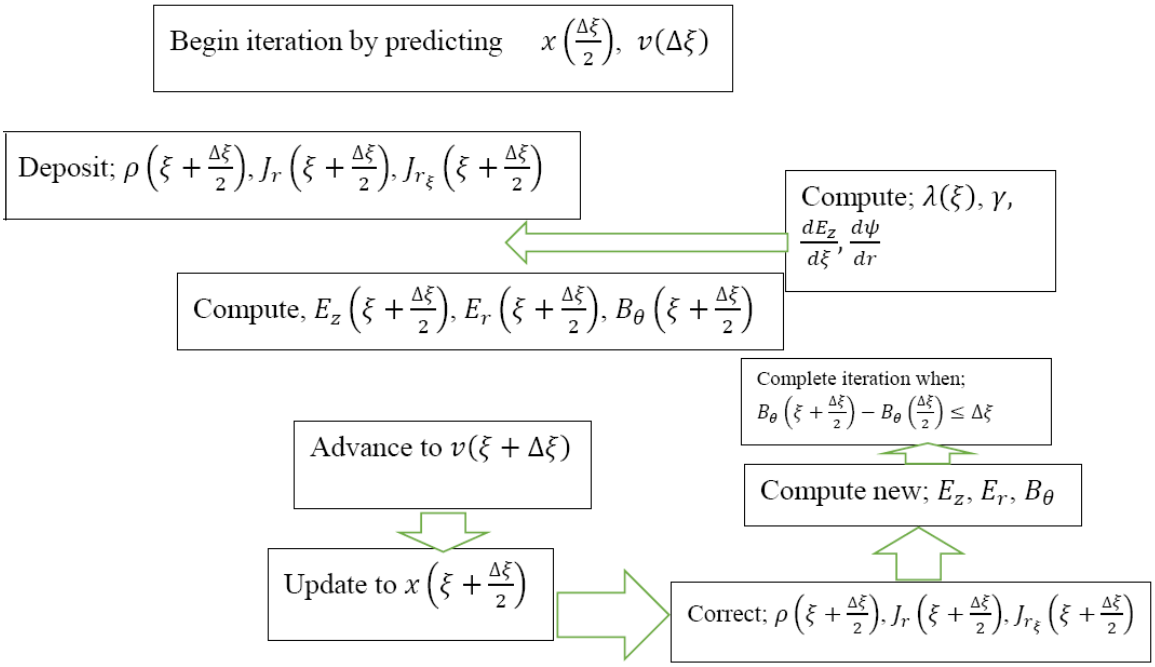

Figure 2: flow chart of the predictor corrector scheme for updating particle positions and fields

E *Plasma Equation of Motion*

The radial equation of motion of the form below is required to advance plasma particles

$$\frac{dP_r}{d\xi}=\frac{qmc^2\gamma_p}{mc^2+q\psi}\frac{\partial\psi}{\partial r}-B_\theta \quad \text{or}$$

$$\frac{dP_r}{d\xi}=q_T\gamma_p\frac{\partial\psi}{\partial r}-B_\theta \qquad (63)$$

equation (63), can be re-expressed as

$$\frac{dP_r}{d\xi}=-q_T\gamma_pE_r+B_\theta\left(q_T\gamma_p-1\right) \qquad (64)$$

For computational ease, the non-relativistic Boris pusher will be used to describe how plasma particles are advanced. Therefore, we recast equation (64) as

$$\frac{du_r}{d\xi}=-\frac{q_T\gamma_p}{m}E_r+\frac{B_\theta}{m}\left(q_T\gamma_p-1\right) \qquad (65)$$

Where we have set $P_r=m\gamma v_r=mu_r$ and $u_r=\gamma v_r$, which implies that we can also have

$$\frac{dr}{d\xi}=\frac{mc^2u_r}{mc^2+q\psi} \qquad (66)$$

Also, it has been shown that the wakefield potential ψ can be evolved (Francesco, 2014) using the relation

$$\frac{d\psi}{d\xi}=\frac{mc^2u_r}{mc^2+q\psi}(E_r-B_\theta)-E_z \qquad (67)$$

F *Numerical Scheme for Plasma Macro Particle Advancement*

In this section, equations (65), (66) and (67) are solved numerically using predictor – corrector scheme, to advance plasma macro particles. To achieve this, the Adams – Bashforth – Moulton predictor – corrector pair is applied. Where the wakefield potential (ψ), macro particle position (r) and velocity (u) will be predicted using Adams – Bashforth formula of order four and letter corrected using Adams – Moulton formula of the same order using predicted previous information. But first, we rewrite equations (65), (66) and (67) as

$$\frac{du_r}{d\xi} = \eta_u = -\frac{q_T\gamma_p}{m}E_r + \frac{B_\theta}{m}\left(q_T\gamma_p - 1\right) \quad (68)$$

$$\frac{dr}{d\xi} = \eta_r = \frac{mc^2u_r}{mc^2+q\psi} \quad (69)$$

and

$$\frac{d\psi}{d\xi} = \eta_\psi = \frac{mc^2u_r}{mc^2+q\psi}(E_r - B_\theta) - E_z \quad (70)$$

So that u_r, r and ψ be evolved numerically as

$$u_{r\varphi_{n+1}} = u_{r\varphi_n} + \frac{\Delta\xi}{24}\left[55\eta_{u_n} - 59\eta_{u_{n-1}} + 37\eta_{u_{n-2}} - 9\eta_{u_{n-3}}\right] \quad (71)$$

And

$$\tilde{u}_{r\varphi_{n+1}} = u_{r\varphi_n} + \frac{\Delta\xi}{24}\left[9\eta_{u_{n+1}} + 19\eta_{u_n} - 5\eta_{u_{n-1}} + \eta_{u_{n-2}}\right] \quad (72)$$

Also

$$r_{\varphi_{n+1}} = u_{r\varphi_n} + \frac{\Delta\xi}{24}\left[55\eta_{r_n} - 59\eta_{r_{n-1}} + 37\eta_{r_{n-2}} - 9\eta_{r_{n-3}}\right] \quad (73)$$

and

$$\tilde{r}_{\varphi_{n+1}} = u_{r\varphi_n} + \frac{\Delta\xi}{24}\left[9\eta_{r_{n+1}} + 19\eta_{r_n} - 5\eta_{r_{n-1}} + \eta_{r_{n-2}}\right] \quad (74)$$

Lastly,

$$\psi_{n+1} = \psi_n + \frac{\Delta\xi}{24}\left[55\eta_{\psi_n} - 59\eta_{\psi_{n-1}} + 37\eta_{\psi_{n-2}} - 9\eta_{\psi_{n-3}}\right] \quad (75)$$

And

$$\tilde{\psi}_{n+1} = \psi_n + \frac{\Delta\xi}{24}\left[9\eta_{\psi_{n+1}} + 19\eta_{\psi_n} - 5\eta_{\psi_{n-1}} + \eta_{\psi_{n-2}}\right] \quad (76)$$

The error estimate is given as

$$\varepsilon_{n+1} = -\frac{19}{270}\left(\tilde{u}_{r_{n+1}} - u_{r_{n+1}}\right)$$

Clearly, a starting technique is required for implementing these equations. Therefore, the 4th order Runge-Kutta (RK4) method is employed, since we are using 4th order multistep method as our predictor – corrector scheme.

G *Beam Particles Advancement Scheme*

In quasi static approximation, the beam is advanced using a different time variable, defined (Morshed *et al.* 2010) as $s = ct$. Therefore, it is necessary to express the set of equations describing the beam evolution in s. To achieve this, we proceed as

$$\frac{\partial s}{\partial t} = c \quad \Longrightarrow \partial t = \frac{\partial s}{c} \quad (77)$$

Lorentz force equation is required to describe the beam evolution through plasma

$$\frac{\partial P_b}{\partial t} = q_b\left[E + \frac{v_b}{c} \times B\right] \quad (78)$$

Using equation (456), equation (457) will become

$$\frac{\partial P_b}{\partial s} = \frac{q_b}{c}\left[E + \frac{v_b}{c} \times B\right] \quad (79)$$

This work considered highly relativistic beam models, so $v_b = c$. Which therefore imply that the radial and longitudinal evolution of the beam particles can be express as

$$\frac{\partial P_{r_b}}{\partial s} = \frac{q_b}{c}E_r \quad (80)$$

$$\frac{\partial P_{z_b}}{\partial s} = \frac{q_b}{c}E_z \quad (81)$$

Using the relation $u = \gamma v$, equations (80) and (81) will become

$$\frac{\partial u_{r_b}}{\partial s} = \frac{q_b}{mc}E_r \quad (82)$$

$$\frac{\partial u_{z_b}}{\partial s} = \frac{q_b}{mc}E_z \quad (83)$$

And the beam particles positions are advanced as

$$\frac{dx_b}{ds} = \frac{u_{x_b}}{\gamma_b} \quad (84)$$

$$\frac{dy_b}{ds} = \frac{u_{y_b}}{\gamma_b} \quad (85)$$

The relation $\xi_b = ct - z$ is used to get

$$\frac{d}{dt}\xi_b = c - v_b \quad (86)$$

Using equation (77), equation (86) can then be expressed as

$$\frac{d}{ds}\xi_b = 1 - \frac{v_{z_b}}{c} \quad \text{or}$$

$$\frac{d}{ds}\xi_b = 1 - \frac{u_{z_b}}{\gamma_b c} \quad (87)$$

The numerical form of equations (82), (83), (84), (85) and (87) will be

$$\frac{u_{r_{bn+1}} - u_{r_{bn}}}{\Delta s} = \frac{q_{bn}}{mc}E_{r_{n+\frac{1}{2}}} \quad (88)$$

$$u_{r_{bn+\frac{1}{2}}} = \frac{u_{r_{bn+1}} + u_{r_{bn}}}{2} \quad (89)$$

$$\frac{u_{z_{bn+1}} - u_{z_{bn}}}{\Delta s} = \frac{q_{bn}}{mc}E_{z_{n+\frac{1}{2}}} \quad (90)$$

$$x_{b_{n+\frac{1}{2}}} = x_{b_n} + \frac{\Delta s}{2}\frac{u_{x_{bn}}}{\gamma_{b_n}} \quad (91)$$

$$y_{b_{n+\frac{1}{2}}} = y_{b_n} + \frac{\Delta s}{2}\frac{u_{y_{bn}}}{\gamma_{b_n}} \quad (92)$$

$$\xi_{b_{n+\frac{1}{2}}} = \xi_{b_n} + \frac{\Delta s}{2}\left(1 - \frac{u_{z_{bn}}}{c\gamma_{b_n}}\right) \quad (93)$$

III RESULTS AND DISCUSSION

A *Beam and Plasma Particles Representation*

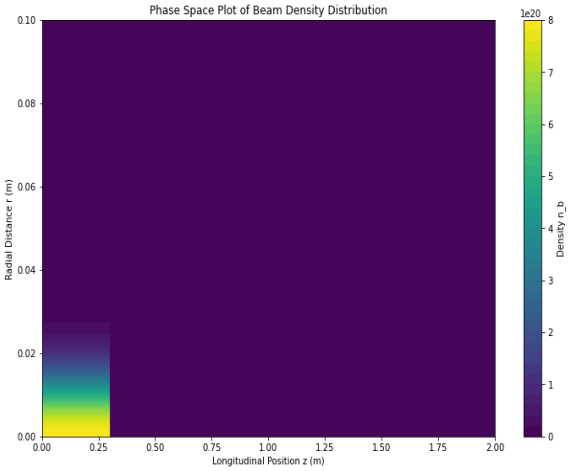

Figure 3: phase space representation of the square beam charge density charge distribution

In Figure 3 above, the yellow to green region indicate where the beam density is largely concentrated. Such that, the beam is highly localized near the front of the simulation domain. The compact nature of the beam is suitable for driving a strong wakefield because the beam density is high where it is concentrated.

Therefore, the phase space plot clearly indicates that the beam is highly localized, focused and ideal for generating strong wakefield when driven in plasma. The narrow radial distribution of the beam suggests a potential of strong focusing force which usually ensure effective interaction with plasma particles. The longitudinal density profile suggest that the beam is compact enough to induce substantial plasma electrons displacement, necessary for large amplitude wakefield or strong wakefield excitation.

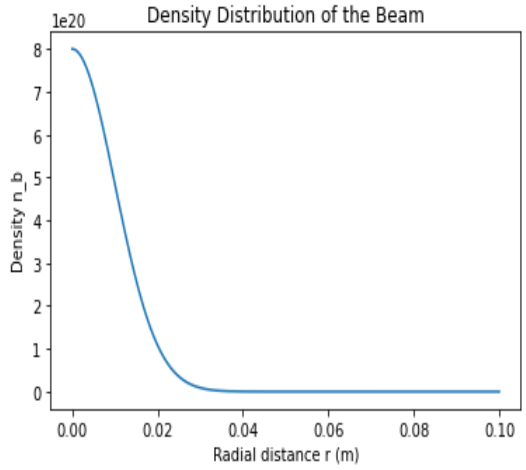

Figure 4: Line plot of the beam charge density distribution with distance

The density distribution of the beam as a function of radial distance r is shown in Figure 4. The beam density n_b reached a peak of $8 \times 10^{20} m^{-3}$ at the radial center, and steeply decrease with increase in r. The radial distance r is the distance away from the center of the beam in meters. This plot indicates that the beam density is highly concentrated near it center (where $r = 0$). The sharp density gradient ensures that the beam interact strongly with the plasma electrons, thereby, largely responsible for creating strong accelerating wakefield behind the beam, as it propagates through the plasma.

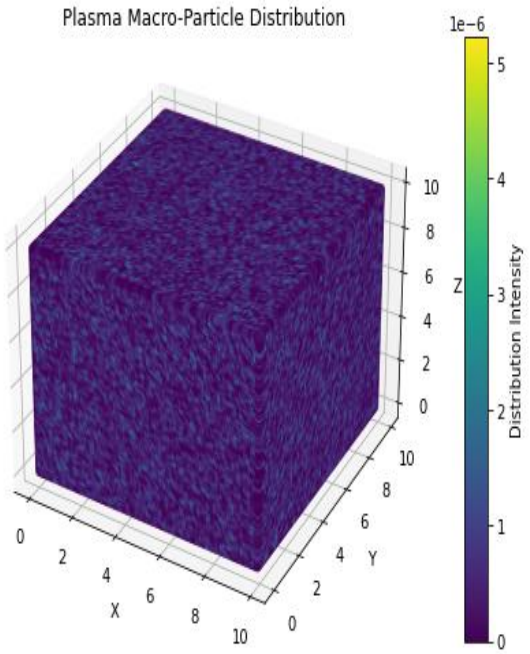

Figure 5: plasma macro-particles distribution in 3-dimension

This represents plasma macro-particle distribution within the specified plasma volume. The dark regions correspond to lower plasma macro particle density while the brighter regions (yellow and green) correspond to regions with higher densities. The plot indicates a slight perturbed plasma macro-particle distribution, as observed from the colour variation seen. They could be as a result of the thermal state of the plasma electrons or non-uniformity in the initial condition applied. However, this basically represent the initial plasma state before propagation of the drive beam through the plasma

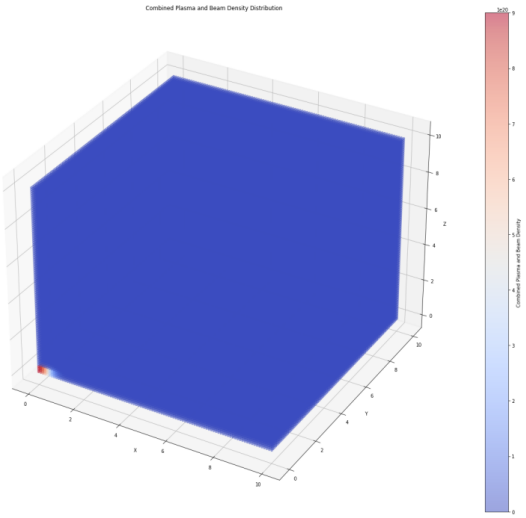

Figure 6: square beam in plasma distribution

The red region shows the high-density particle beam, used as the drive beam in the plasma. The blue regions indicate the unperturbed plasma with low density compared to the high-density beam. This plot depicts the initial stage where the beam is introduced into the plasma.

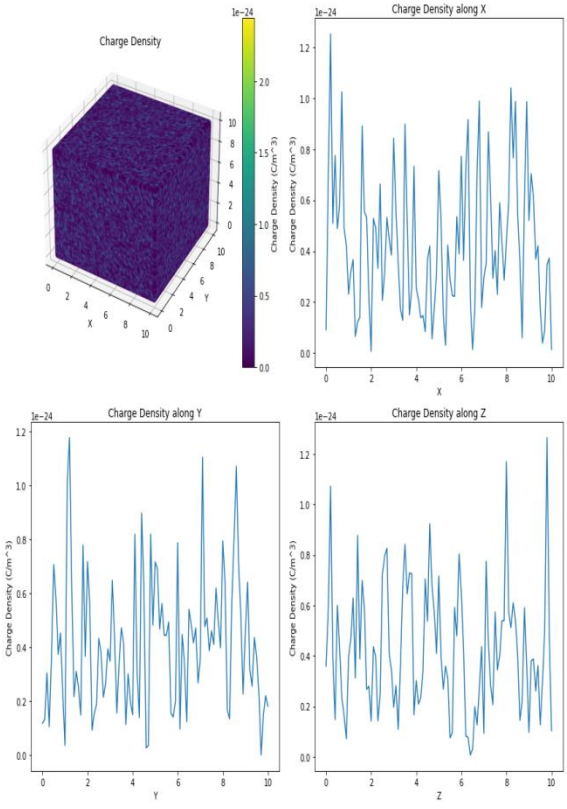

Figure 7: plasma charge density distribution. From left to right, depict plasma particles phase space charge density distribution, charge density distribution along x, y, and z-direction

The 3D charge density distribution (top-left) shows how charge density is distributed spatially through the plasma simulation domain. The charge density distribution appears to be fairly uniform with small variations throughout the simulation domain. The total intensity of the charge density is low, around $1 \times 10^{-24} C/m^3$, which is consistent with charge densities required for plasma simulations.

The plots in top-right, bottom-right, and bottom-left exhibit similar fluctuations in charge density between 0 and $1.2 \times 10^{-24} C/m^3$. These oscillations observed could be due to the slight perturbation effects observed could be due to the slight perturbations seen in Figure 5. The anisotropy in charge density oscillations along different axes, suggest that the wakefield generation has direction-dependent effects.

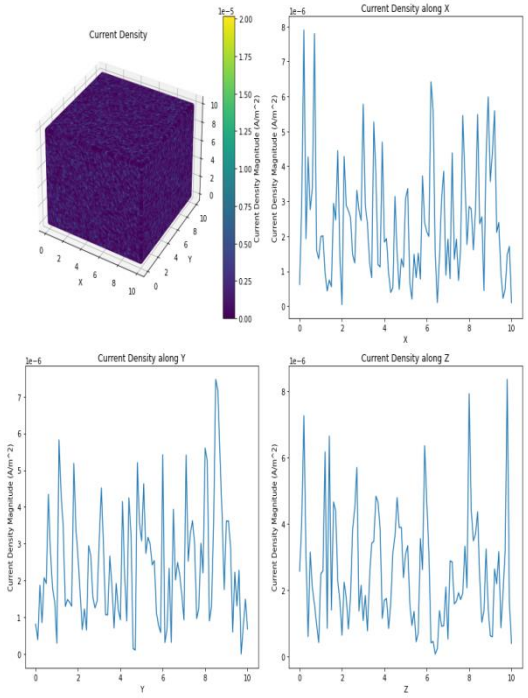

Figure 8: plasma current density distribution. From left to right, depict plasma particles phase space current density distribution, charge current distribution along x, y, and z-direction

The top-right plot illustrates the spatial distribution of the current density across the simulation domain. The magnitude of the current density is approximately $2 \times 10^{-5} A/m^2$, as indicated by the color bar, suggesting that the plasma current density is relatively small. The plots also reveal a non-uniform distribution with localized regions of high current density amidst areas of lower density, highlighting the flow of charges within the plasma. However, the significance of current density on the normalized

blowout radius has been mentioned (Lu *et al.,* 2010). Consequently, the potential applications of high average current density generated in a plasma accelerator has been stressed (Zgadgaj *et al.,* 2020).

IV CONCLUSION

This progress report highlights the successful development of a quasi-static PIC code tailored for nonlinear beam-driven PWFA simulations. The achieved reductions in computational complexity, coupled with the accurate representation of beam-plasma dynamics, position the code as a valuable asset for advancing plasma accelerator research. Continued efforts in validation, optimization, and feature integration will further solidify its role in pushing the boundaries of plasma-based acceleration technologies, ultimately contributing to the realization of more compact, efficient, and powerful particle accelerators.

ACKNOWLEDGMENT

We appreciate Tertiary Education Trust Fund (TETFund) for funding this research work

REFERENCES

[1] Francesco, R. (2014). Numerical and Analytical Methods for Laser-Plasma Acceleration Physics. PhD Dissertation. Department of Physics. University of Bologna. Italy. 134pp.

[2] Gangtak, N. Echi, I.M. Mairiga, A.J. Hemba, E.C. and Trisma E.A. (2017). Scaling of Transformer Ratio and Energy Gain in a Plasma Wakefield Acceleration Scheme Driven by Positron Beam. Advances in Physics Theories and Applications. 64: 1 – 15.

[3] Gangtak, N., Anchaver, R. S., and Echi, I. M. (2016). Simulation of Positron Beam Driven Plasma Wakefield Acceleration using the Particle – in – Cell Code in Metre – Scale Plasma. Journal of the Nigerian Association of mathematical physics. 34: 323 – 330

[4] Haruna, M.A. and Anchaver, R.S. (2013). Simulation of Position Beam Driven Plasma Wakefield Acceleration using the Particle-in-Cell Code, OOPIC. Journal of the Nigerian Association of mathematical Physics. 25: 129-134

[5] Lapenta G. (2015). Kinetic Plasma Simulation: Particle in Cell Method. Retrievable from: https://www.researchgate.net/publication/2801

[6] Litos, M. Adli, E. An, W. Clark, C.I. Corde, S. Clayton, C.E. Frederico, J. and Green, S.Z. (2016). 9GeV Energy Gain in a Beam Driven Plasma Wakefield Accelerator. Plasma Physics and Controlled Fusion. 58: 034017-1 – 034017-6

[7] Massimo, F. Marocchino, A. Chiadroni, E. Ferrario, M. Mostacci, A. Musumeci,P. and Palumbo, L. (2013). Transformer Ratio Studies for Single Bunch Plasma Wakefield Acceleration. Nuclear Instruments and Methods in Physics Research A

[8] Pukhov, A. (2015). Particle-in-Cell Codes for Plasma Based Particle Acceleration. Retrieved from:http://arXiv:1510.01071v1[physics. plasma-ph]

[9] U.S. Department of Energy (2016). Advanced Accelerator Development Strategy Report. Retrieved from; http://science.energy.gov/~/media/hep/hepap/pdf/Reports/Accelerato -RD Subpanel-Reportpdf

[10] Wojciech, K. (2017). Particle-in-Cell Electrostatic Numerical Algorithm. Transactions of the Institute of Aviation – Sciendo. 3(248): 24 – 45

[11] Morshed, S. Antonsen, T.M. and Palastro, J.P. (2010). Efficient Simulation ofElectron Trapping in Laser and Plasma Wakefield Acceleration. Retrieved from: http://link.aip.org/link/?PHP/17/063106/1

[12] Derouillat, J. Beck, A. Perez, F. Vinci, T. Chiaramello, M. Grassi, A. Fle', M.Bouchard, Plotnikov, I. Aunai, N. Dargent, J. Riconda, C. and Grech,M.(2017). SMILEI: A Collaborative, Open-Source, Multi-purpose Particle-in Cell Code for Plasma Simulation. Retrieved from: https://arXiv:1702.05128v1[physics.plasm-ph].

[13] Petri, J. (2017). A Fully Implicit Numerical Integration of the Relativistic Particle Equation of Motion. Retrieved from: http://arXiv:1612.04563v2[physics.plasma-ph]

[14] Diederichs S., Benedetti C., Huebl A., Lehe R., Myers A., Sinn A., Vay J.-L., Zhang and W., Thevenet M. (2022). HiPACE++: A portable 3D quasi-static particle-in-cell code.

Computer Physics Communications 278. 1 – 9.

[15] Zgadzaj R., Silva T., Khudyakov V. K., Sosedkin A., Allen J., Gessner S., Li Z., Litos M., Vieira J., Lotov K. V., Hogan M. J., Yakimenko V., and Downer M. C. (2020). Dissipation of electron-beam-driven plasma wakes. Nature Communications. 4753, 1 – 11.

[16] Lu W., An W., Zhou M., Joshi C., Huang C. and Mori W. B. (2010). The optimum plasma density for plasma wakefield excitation in the blowout regime. New Journal of Physics. 085002. Pp 1-8